

Supplementary Information

**c-di-AMP binds the *ydaO* riboswitch in
two pseudo-symmetry-related pockets**

Aiming Ren¹ & Dinshaw J. Patel^{1,*}

¹Structural Biology Program
Memorial Sloan-Kettering Cancer Center
New York, NY 10065, USA

* email: pateld@mskcc.org

Supplementary Results

Supplementary Table 1. Crystallographic statistics for *T. tengcongensis ydaO* riboswitch with bound c-di-AMP and c-di-dAMP.

Crystal	c-di-AMP -bound	c-di-AMP soaked with [Ir(NH ₃) ₆] ³⁺	c-di-dAMP -bound	c-di-AMP soaked with Mn ²⁺
Data collection	24-ID-E	X29A	24-ID-E	24-ID-C
Space group	C222 ₁	C222 ₁	C222 ₁	C222 ₁
Cell dimensions				
<i>a, b, c</i> (Å)	79.3, 88.2, 145.7	78.4, 88.3, 145.1	77.9, 87.1, 144.6	79.3, 88.1, 145.7
α, β, γ (°)	90, 90, 120	90, 90, 120	90, 90, 120	90, 90, 120
		<i>Peak</i>		
Wavelength	0.9792	1.1052	0.9792	1.7712
Resolution (Å)	50.0-2.73 (2.83-2.73)*	50.0-2.90 (3.0-2.90)	144-2.65 (2.79-2.65)	145.7-3.57 (3.76-3.57)
<i>R</i> _{pim} or <i>R</i> _{merge}	0.033 (0.725)	0.066(0.99)	0.047 (0.722)	0.074 (0.584)
<i>I</i> / σ <i>I</i>	31 (1.2)	29 (1.5)	17.5 (1.1)	8.1 (1.3)
Completeness (%)	99.7 (100)	99.0 (98.5)	99.7 (100)	97.8 (98.9)
Redundancy	7.2 (7.4)	14.6 (14.9)	7.0 (7.4)	6.1 (6.3)
Refinement				
Resolution (Å)	45.6-2.69		42.3-2.65	72.8-3.6
No. reflections	14169		14520	11531
<i>R</i> _{work} / <i>R</i> _{free}	0.21/0.24		0.22/0.29	0.23/0.30
No. atoms				
RNA	2316		2617	2316
Ligand	88		84	88
Cations	2		2	2
Water	33		7	
B-factors				
RNA	92.2		85.1	100.2
Ligand	73.6		57.6	82.3
Cations	79.1		83.3	48.1
Water	96.9		85.6	
R.m.s deviations				
Bond lengths (Å)	0.010		0.015	0.02
Bond angles (°)	1.698		1.820	1.90

*Values for the highest-resolution shell are in parentheses.

Supplementary Table 2. ITC-based binding parameters for complex formation between c-di-AMP and *T. tengcongensis* ydaO riboswitch as a function of added cyclic dinucleotides and divalent cations.

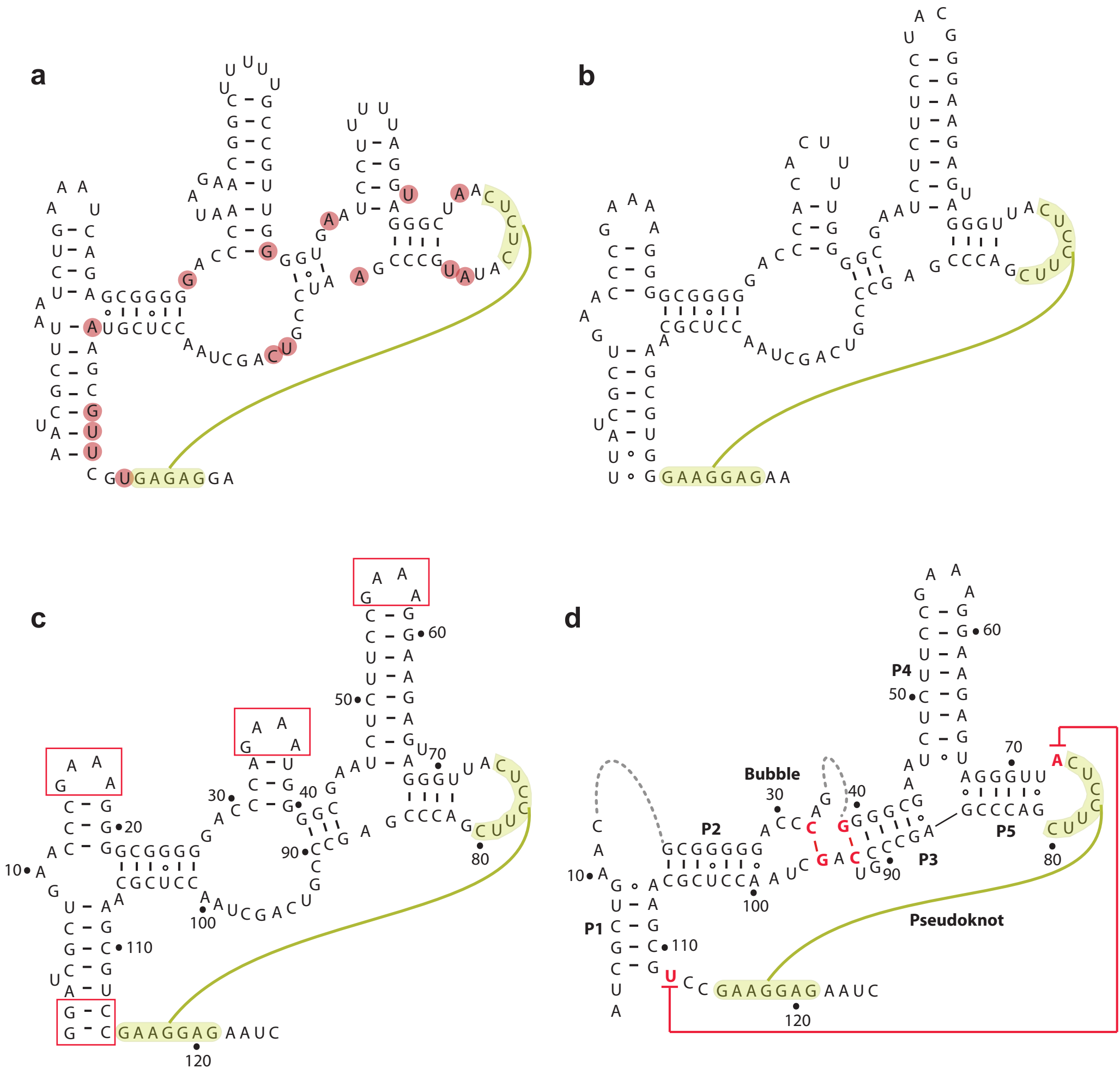
RNA, 5 mM Mg ²⁺ Ligand	ΔH Kcal/mol	ΔS cal/mol/deg	N	Kd μM
c-di-AMP	- 7.7 \pm 0.1	+ 7.9	1.8 \pm 0.02	0.066 \pm 0.02
c-di-dAMP	- 7.4 \pm 0.4	+ 1.3	2.0 \pm 0.08	2.9 \pm 0.8
c-di-GMP	--	--	--	--
c-di-IMP	--	--	--	--
3'3'-cGAMP	--	--	--	--
2'3'-cGAMP	--	--	--	--
2'2'-cGAMP	--	--	--	--

RNA, c-di-AMP mM Mg²⁺	ΔH Kcal/mol	ΔS cal/mol/deg	N	Kd μM
1	- 11.3 \pm 0.3	- 7.7	1.6 \pm 0.03	0.5 \pm 0.12
20	- 8.4 \pm 0.1	+ 6.2	1.5 \pm 0.01	0.05 \pm 0.02

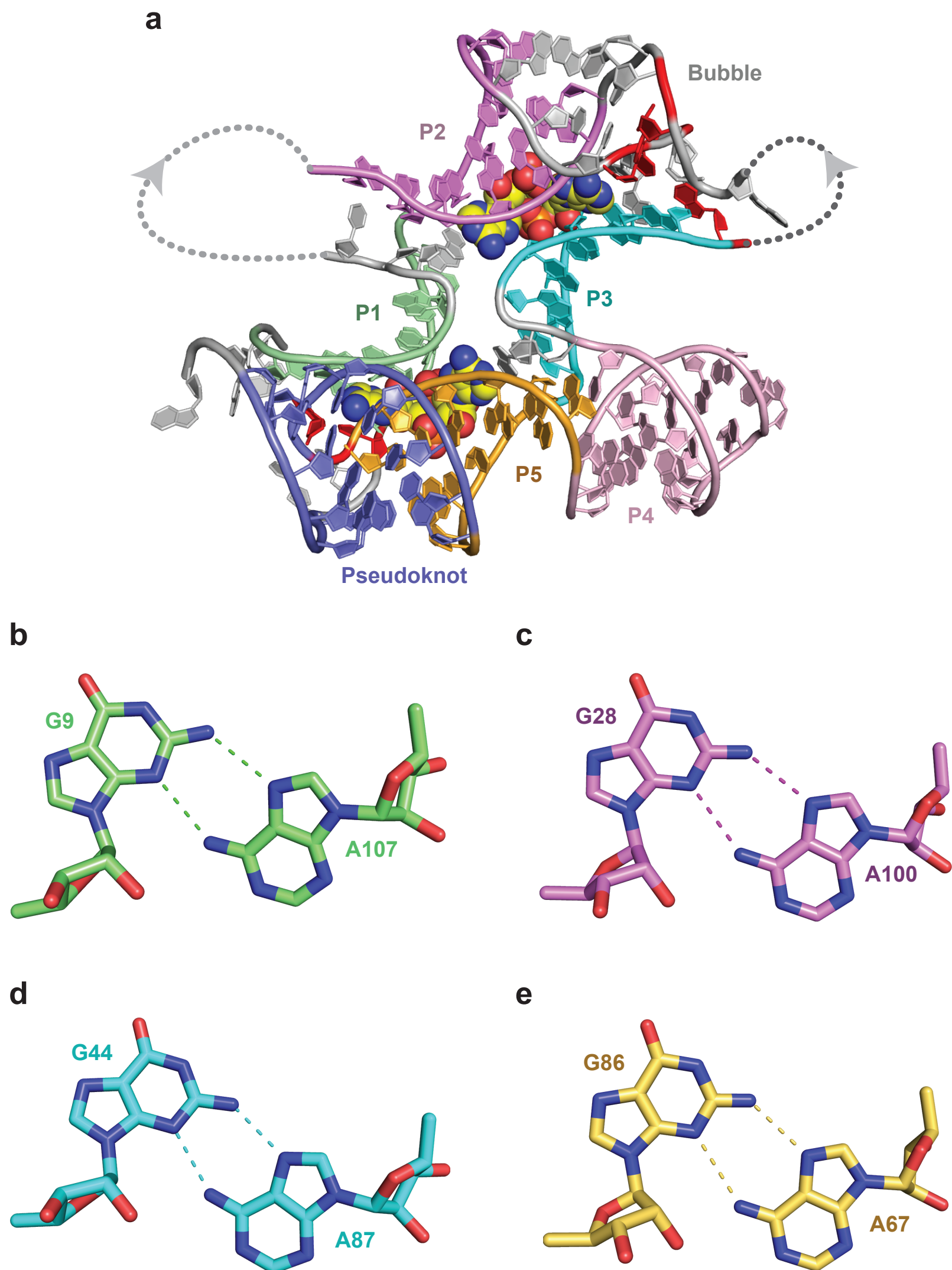
RNA, c-di-AMP 5 mM M²⁺	ΔH Kcal/mol	ΔS cal/mol/deg	N	Kd μM
Mn ²⁺	- 7.5 \pm 0.08	+ 8.3	1.6 \pm 0.01	0.075 \pm 0.02
Ca ²⁺	- 8.4 \pm 0.15	+ 3.0	1.7 \pm 0.02	0.24 \pm 0.06
Ba ²⁺	- 5.9 \pm 0.12	+ 13.1	1.7 \pm 0.02	0.10 \pm 0.04

Supplementary Table 3. ITC-based binding parameters for complex formation between c-di-AMP and the *T. tengcongensis* ydaO riboswitch as a function of mutations of key tertiary interactions.

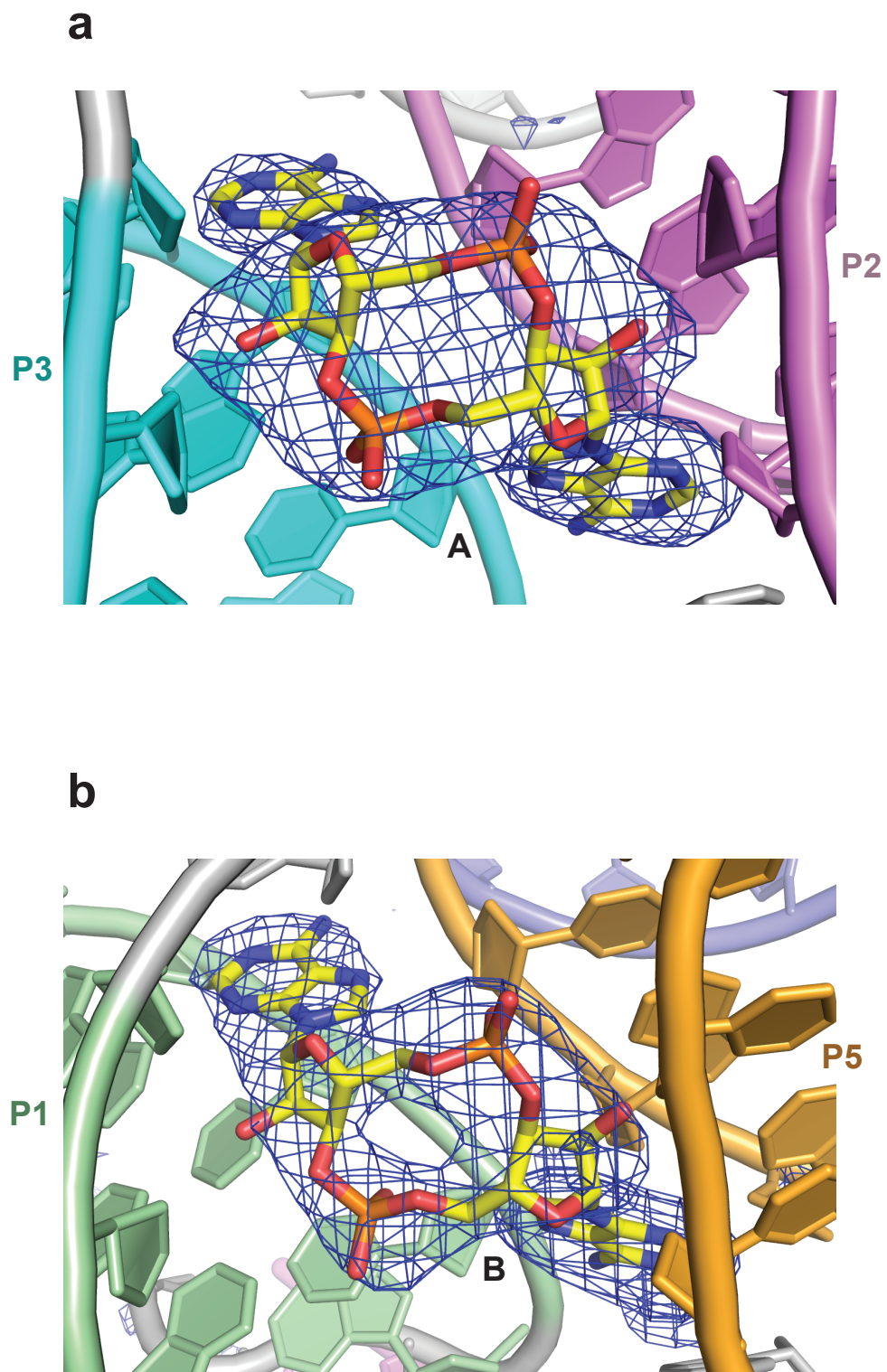
RNA, 5 mM Mg ²⁺ Ligand c-di-AMP Mutant	ΔH Kcal/mol	ΔS cal/mol/deg	N	Kd μM
G39C	- 4.5 \pm 0.3	+ 10.5	1.7 \pm 0.08	3.1 \pm 0.97
A73C	- 4.3 \pm 0.2	+ 11.6	1.5 \pm 0.05	2.8 \pm 0.63
G96C	- 7.9 \pm 0.1	+ 8.5	1.9 \pm 0.01	0.034 \pm 0.02
U98C	--	--	--	--
3AA	- 4.2 \pm 0.2	+ 10.8	1.5 \pm 0.06	4.5 \pm 0.90
3CC	- 3.1 \pm 0.9	+ 11.6	1.5 \pm 0.33	19.8 \pm 9.29
A10C	- 7.7 \pm 0.1	+ 4.5	1.5 \pm 0.02	0.36 \pm 0.07
A45C	- 4.5 \pm 0.1	+ 15.7	1.9 \pm 0.02	0.24 \pm 0.06
A95C	- 6.4 \pm 0.5	+ 3.9	1.4 \pm 0.08	3.9 \pm 1.04



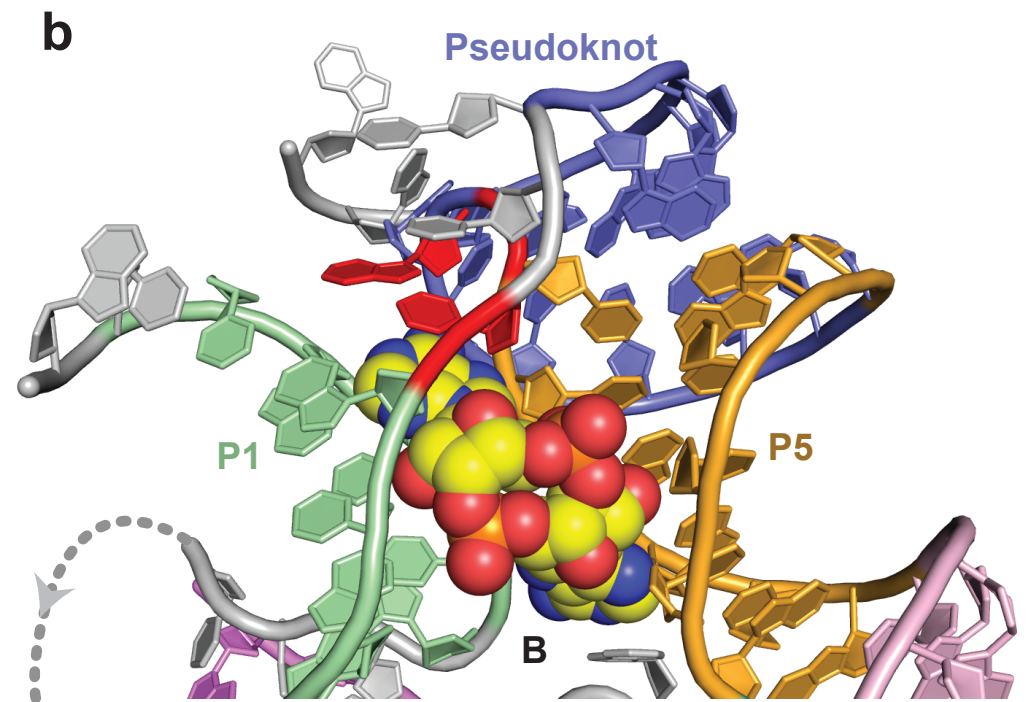
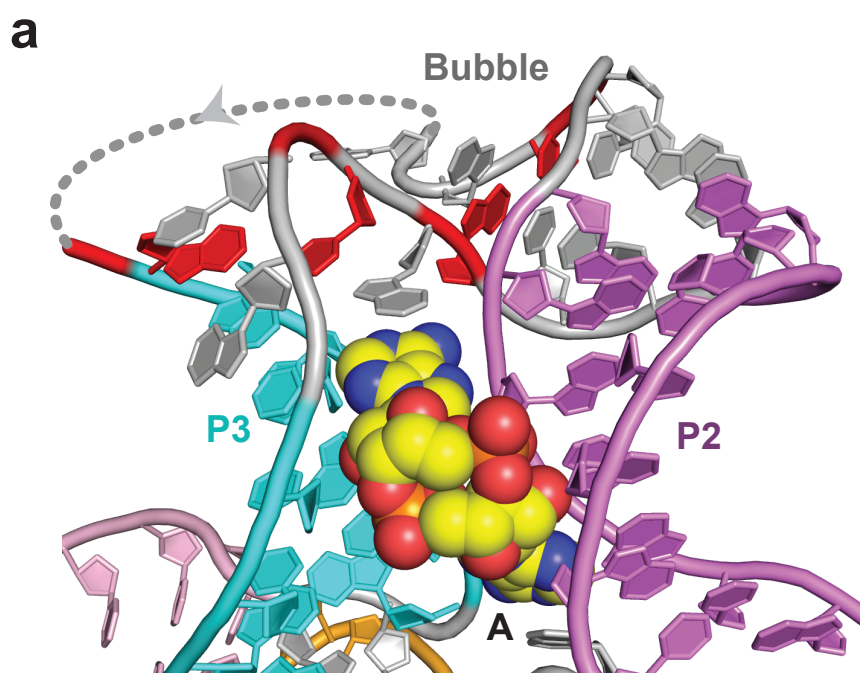
Supplementary Figure 1 | Secondary structures of the sensing domains of the c-di-AMP-binding *ydaO* riboswitches from *B. subtilis* and *T. tengcongensis*. **a**, Secondary structure of the sensing domain of the *B. subtilis ydaO* riboswitch²⁰. Red-labeled nucleotides were protected during in-line probing on addition of c-di-AMP²⁰. **b**, Secondary structure of the sensing domain of the *T. tengcongensis ydaO* riboswitch. **c**, Modifications (shown in red boxes) of the secondary structure of the sensing domain of the *T. tengcongensis ydaO* riboswitch (panel b) to facilitate *in vitro* transcription and crystallization. **d**, Secondary structure as elucidated from the crystal structure of the *T. tengcongensis ydaO* riboswitch with bound c-di-AMP.



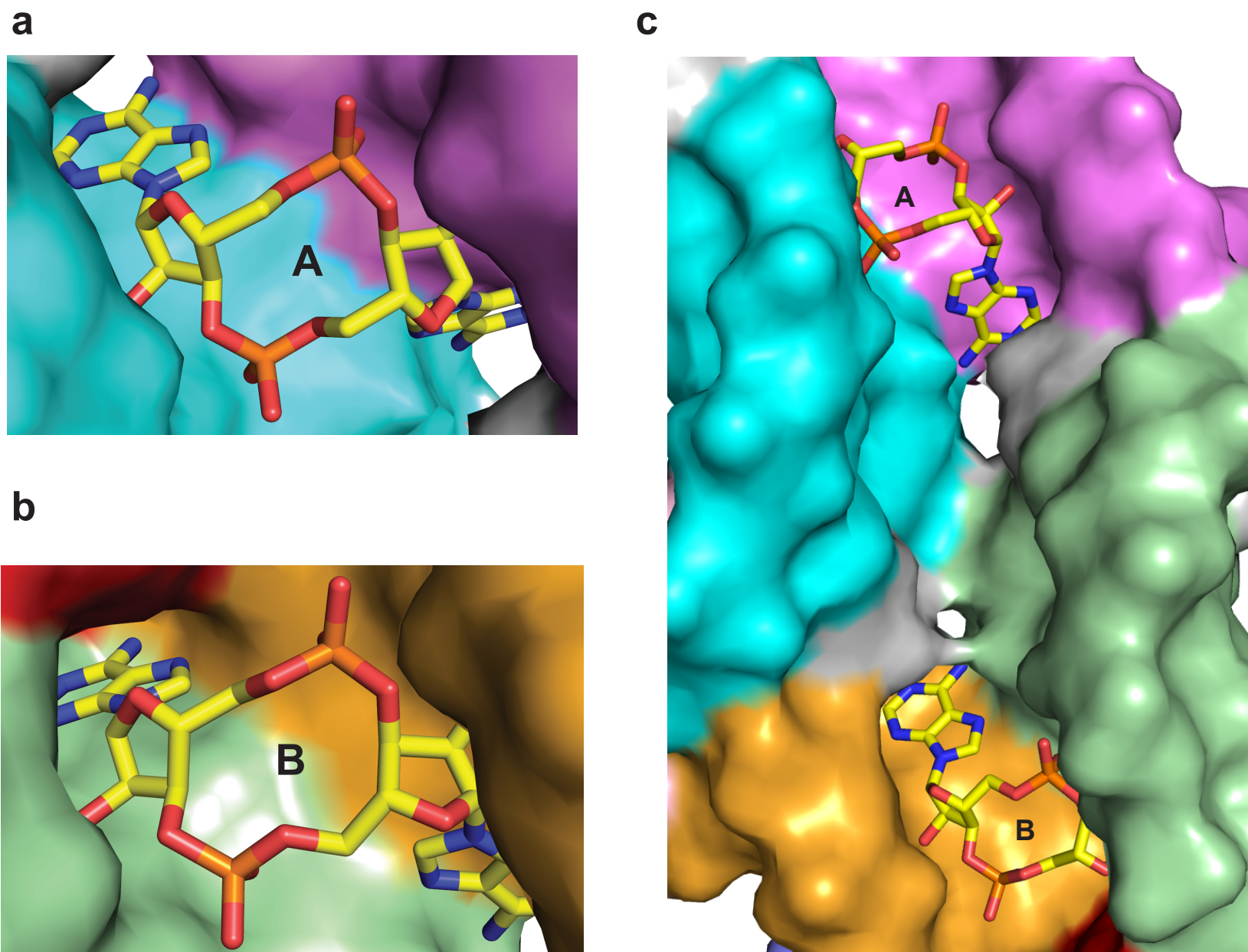
Supplementary Figure 2 | An alternate view of the crystal structure of the *T. tengcongensis* *ydaO* riboswitch bound to two molecules of c-di-AMP, together with alignment of terminal sheared G•A pairs. a, This view is rotated 180 degrees along the vertical axis relative to the structure shown in Fig. 1b. b-e, Four terminal sheared G•A pair alignments in the structure of the complex.



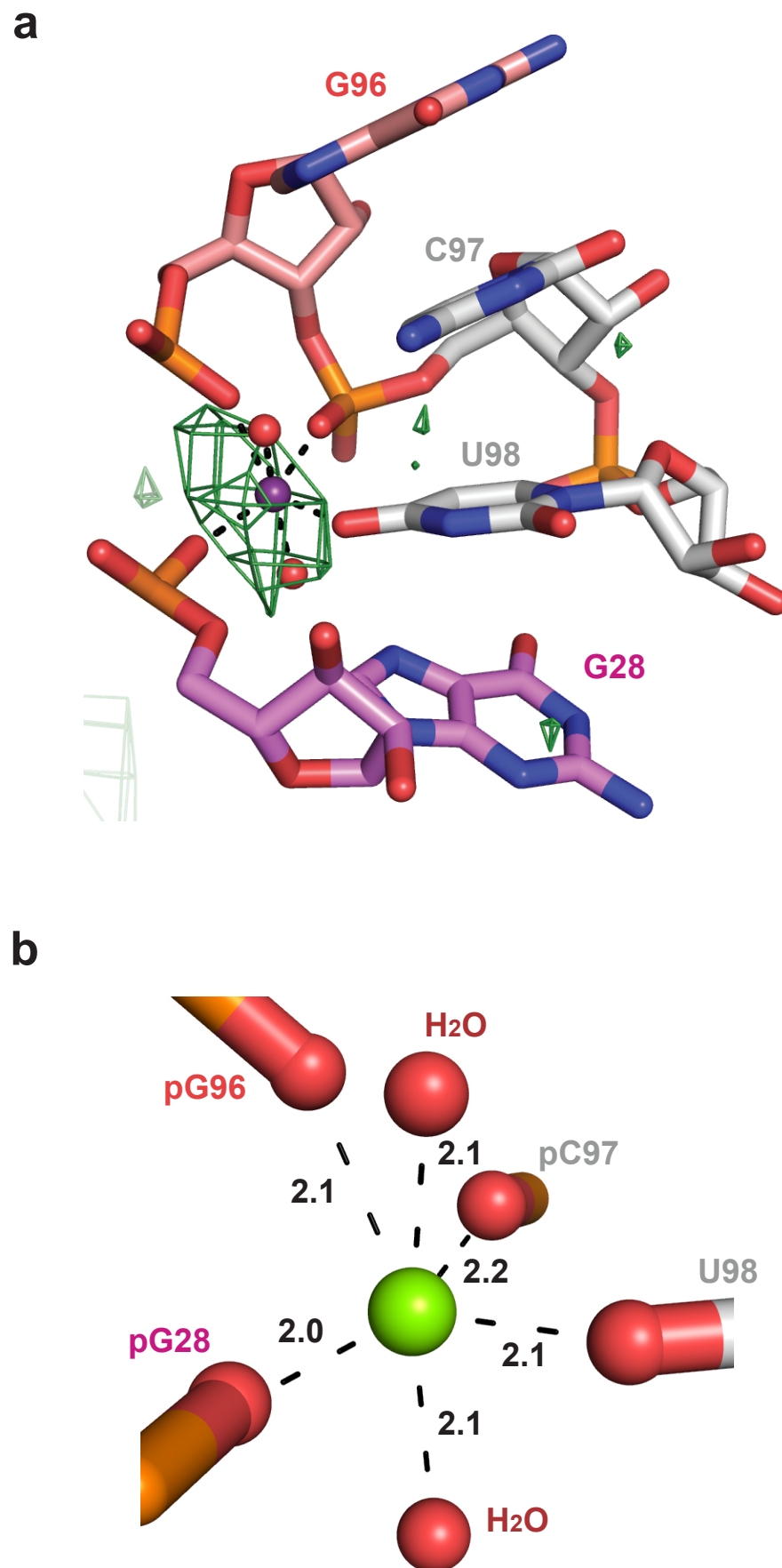
Supplementary Figure 3 | Omit maps of bound c-di-AMP molecules in the structure of the *T. tengcongensis ydaO* riboswitch. a, b, Omit maps (3.0 σ) of bound c-di-AMP molecule A (panel a) and molecule B (panel b) in the structure of the c-di-AMP riboswitch.



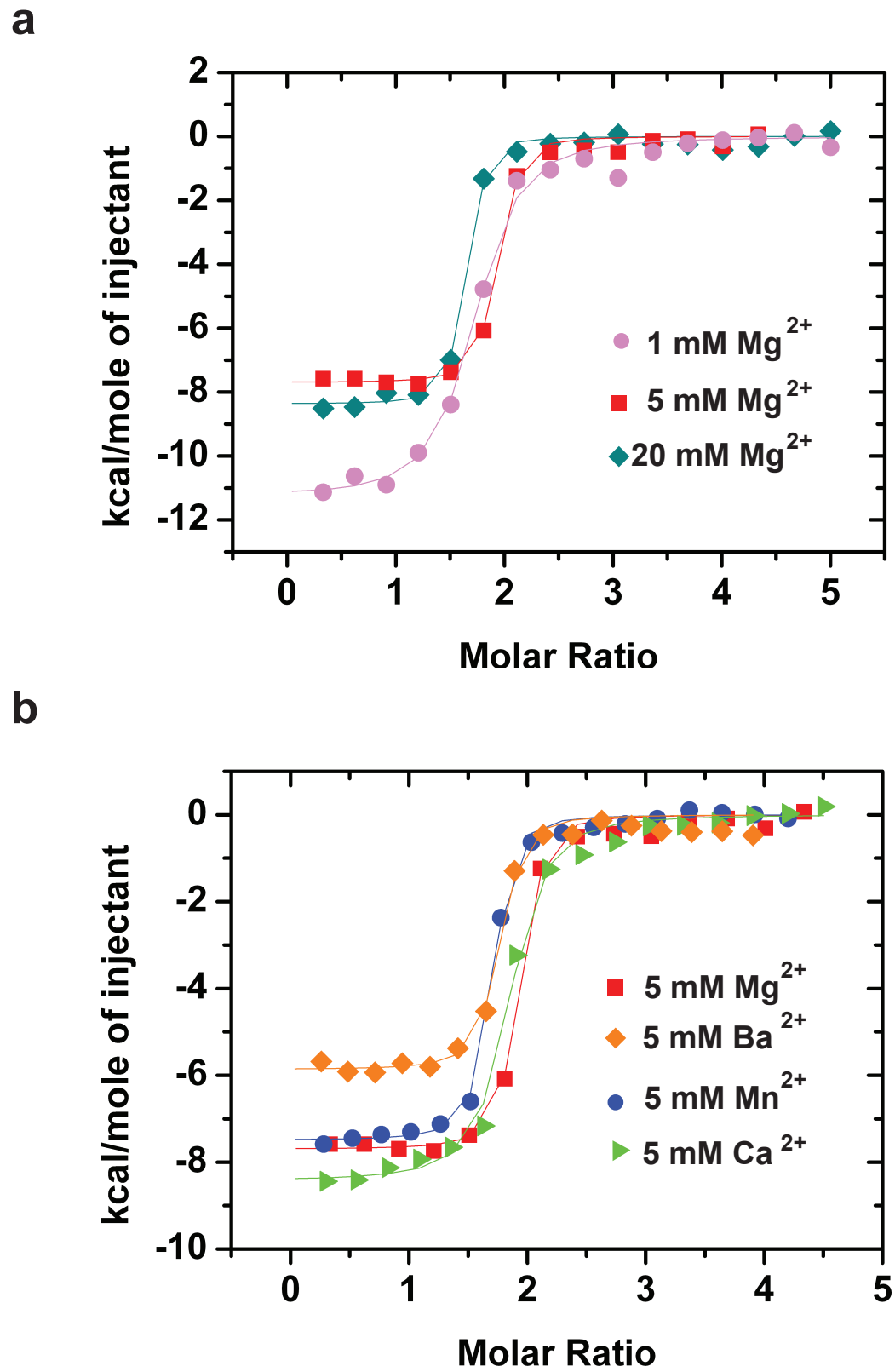
Supplementary Figure 4 | Expanded view of two c-di-AMP binding pockets **a**, An expanded view of c-di-AMP molecule A bound in a pocket formed by stems P2, P3 and the bubble segment. **b**, An expanded view of c-di-AMP molecule B bound in a pocket formed by stems P1, P5 and the pseudoknot segment.



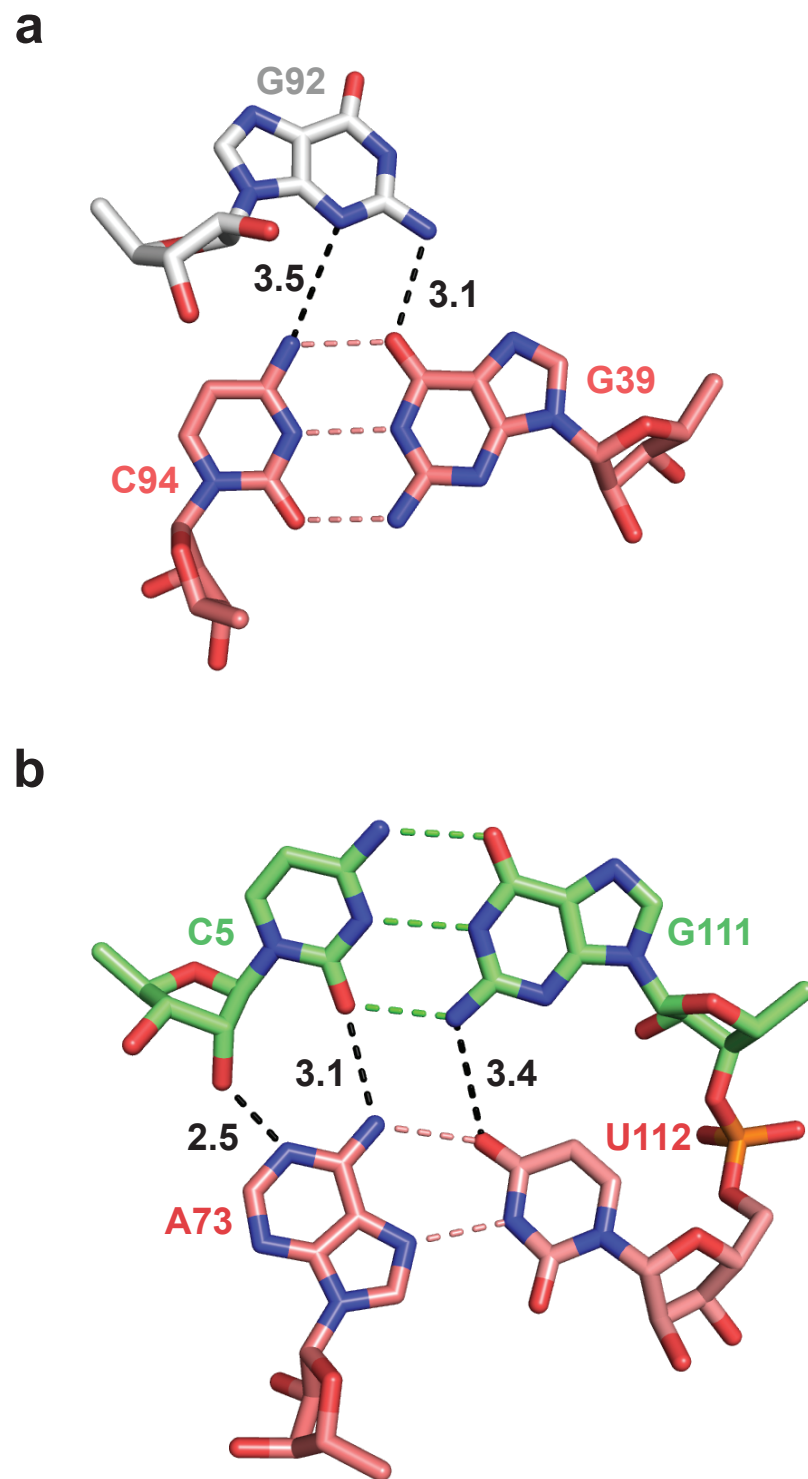
Supplementary Figure 5 | Insertion of the adenine rings of c-di-AMP into both binding pockets in the *ydaO* riboswitch and the segment connecting binding pockets in the structure of the complex. a, b, Insertion of both adenine rings of c-di-AMP molecules A (panel a) and B (panel b) into binding pockets in *ydaO* riboswitch complex. The riboswitch is shown in a surface representation and color-coded by segments as shown in Fig. 1a. c, Depiction of the segment connecting c-di-AMP binding pockets in the structure of the complex.



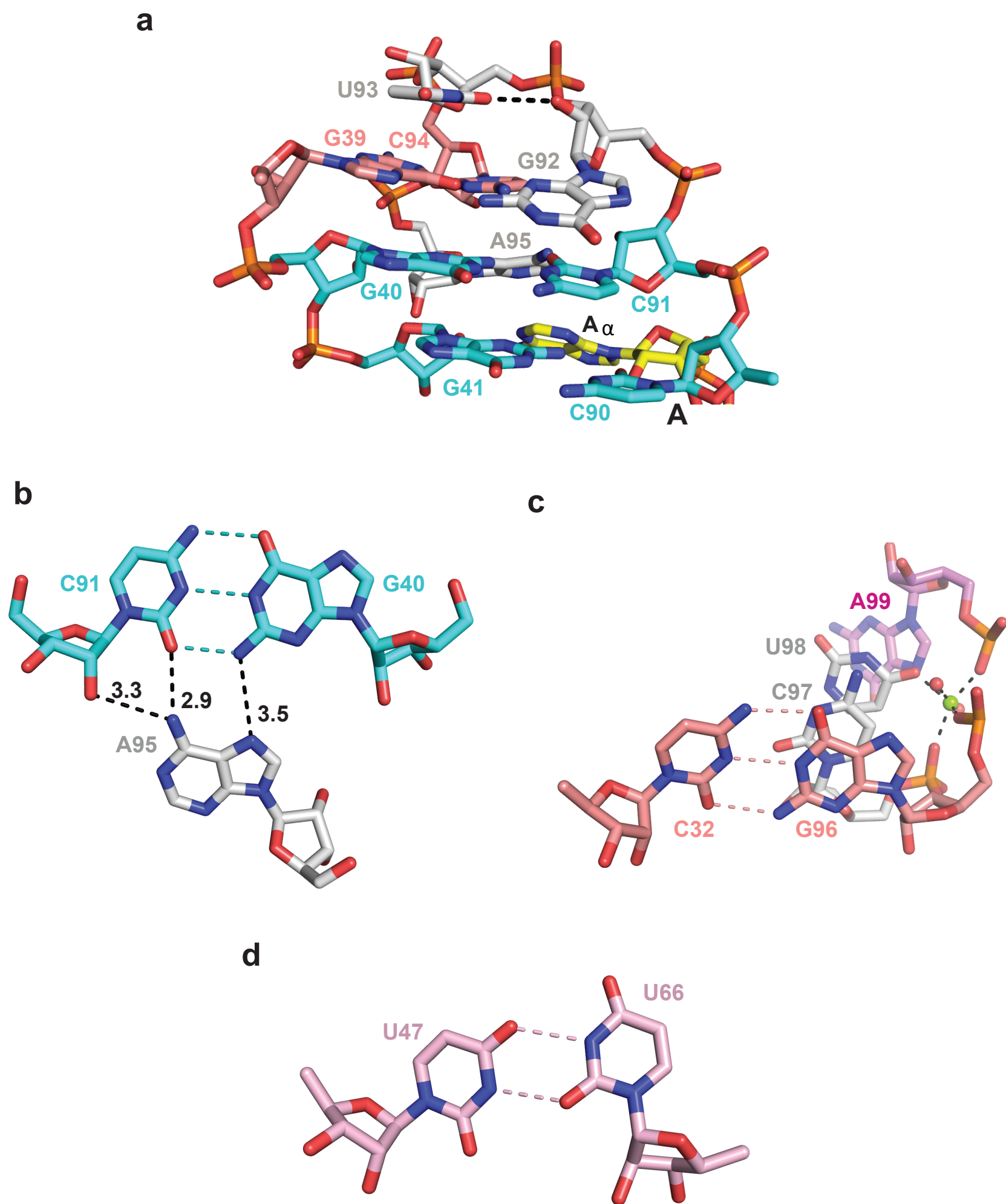
Supplementary Figure 6 | The structure of the *T. tengcongensis ydaO* riboswitch-sensing domain in the bound state in the presence of Mn²⁺ cation. **a, An expanded view of the bound Mn²⁺ cation-binding site in the *ydaO* riboswitch, with the Mn²⁺ anomalous electron density map contoured at 3 σ level. The Mn²⁺ cation and bound water molecules are shown as purple and red spheres. **b**, Bond distances (in Å) between the divalent cation and the coordinating residues of the alignment shown in panel a in the structure of the complex.**



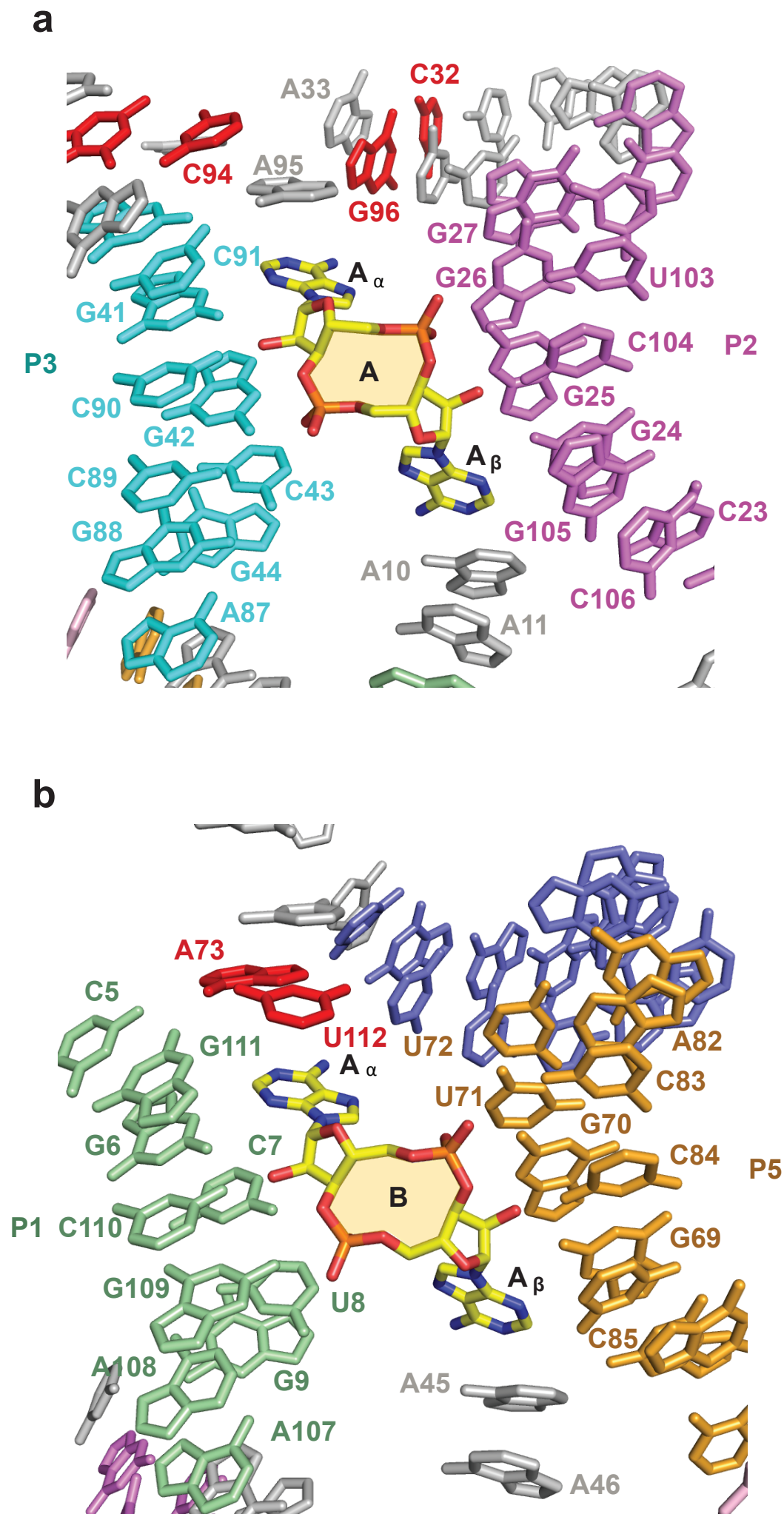
Supplementary Figure 7 | ITC binding curves for titration of *T. tengcongensis ydaO* riboswitch with added c-di-AMP as a function of divalent cations. **a, ITC binding curves of complex formation as a function of Mg²⁺ cation concentration. **b**, ITC binding curves of complex formation as a function of 5 mM Mg²⁺, Mn²⁺, Ba²⁺ and Ca²⁺ cations. In panels a and b, c-di-AMP was added gradually to the *T. tengcongensis ydaO* riboswitch.**



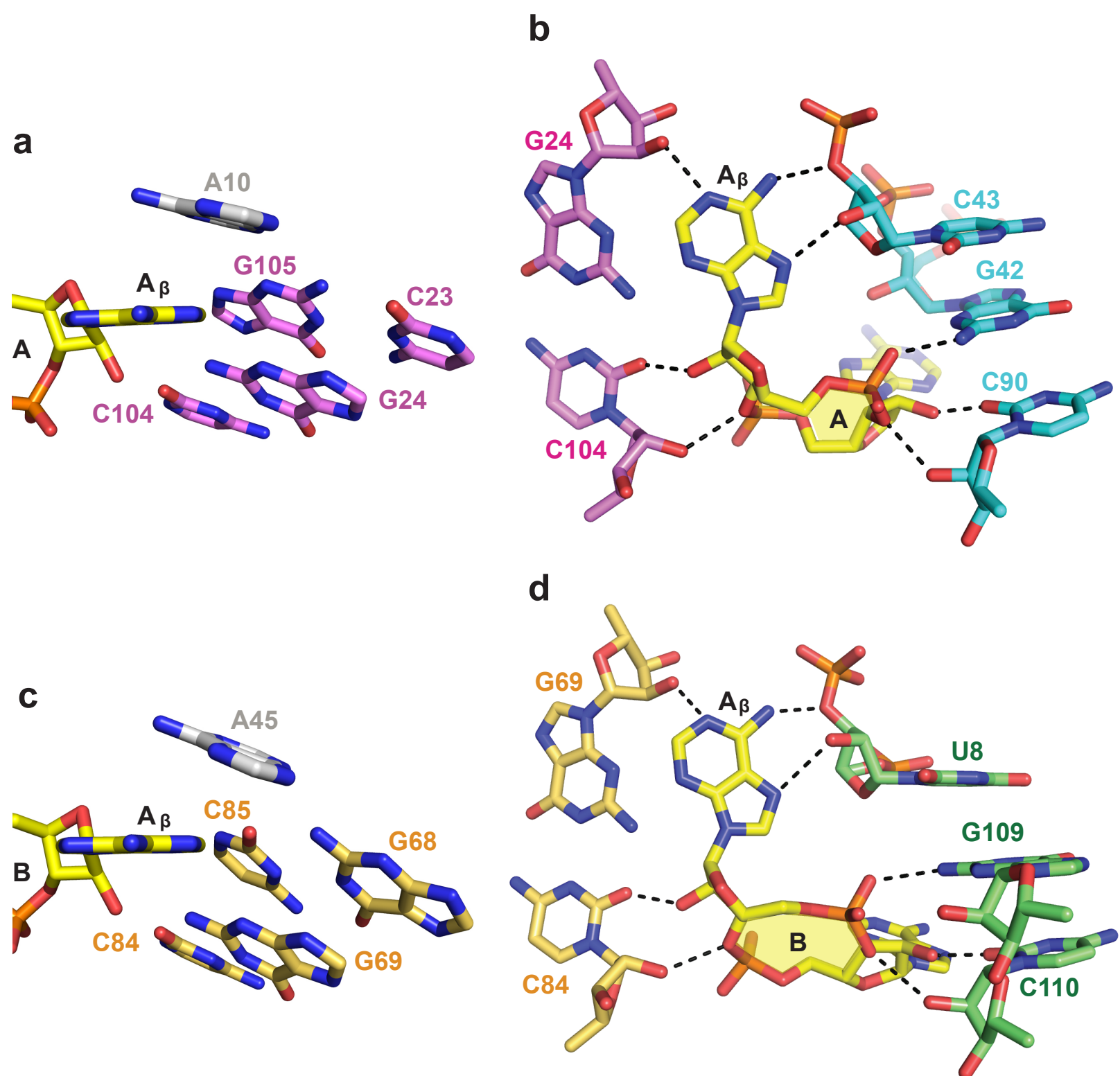
Supplementary Figure 8 | Hydrogen bond distances for key tertiary pairing alignments in the structure of the c-di-AMP bound state of the *T. tengcongensis ydaO* riboswitch. **a, Hydrogen bond distances (in Å, heteroatom to heteroatom) for the major groove base triple formed between G92 and the G39(*anti*)-C94(*syn*) pair. **b**, Hydrogen bond distances for the base tetrad formed by the long-range Hoogsteen A73•U112 pair aligning with the minor groove edge of the Watson-Crick C5-G111 pair.**



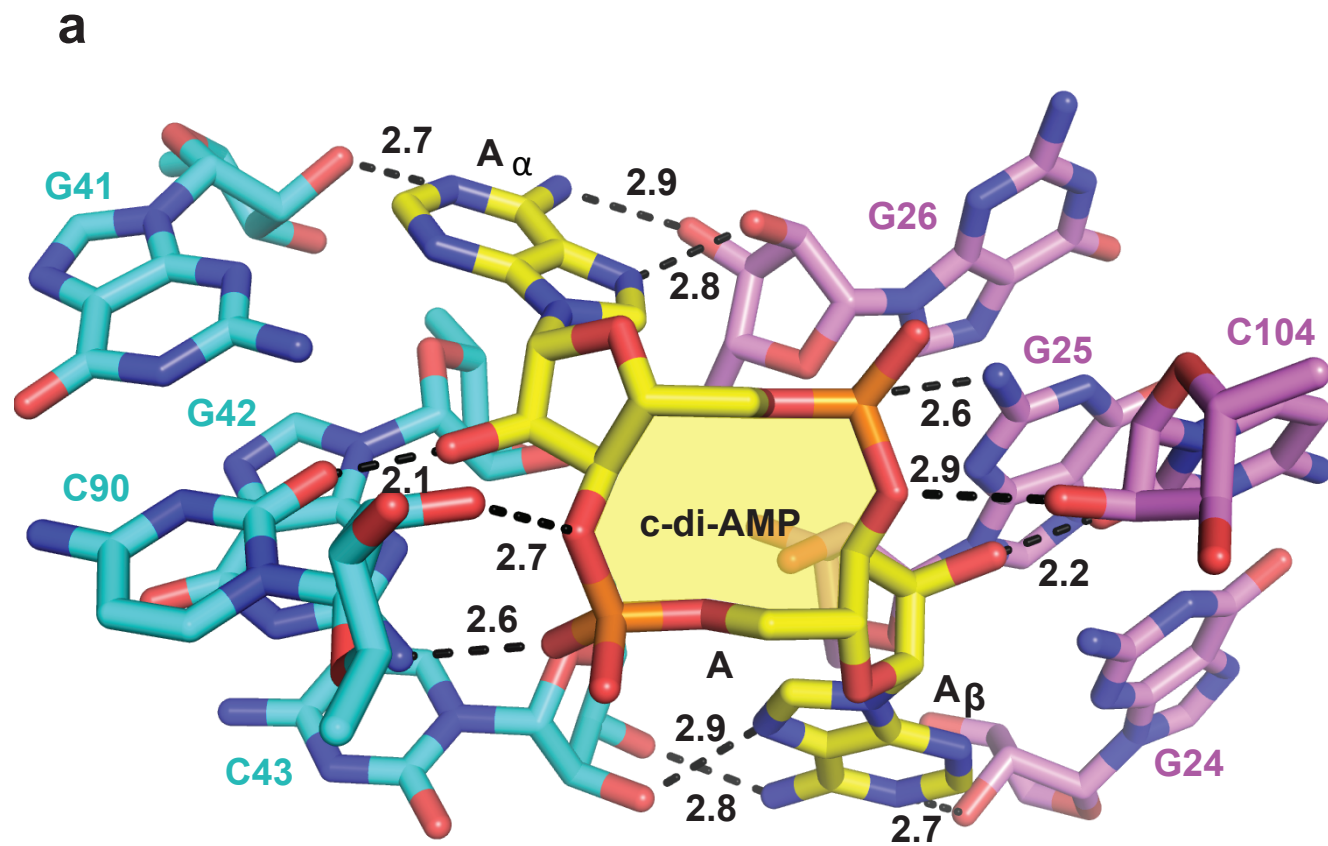
Supplementary Figure 9 | Higher order pairing alignments associated with c-di-AMP binding pocket A and flanking segments composed of helices P2 and P3 and bubble domain of the bound state of the *T. tengcongensis ydaO* riboswitch, together with alignment of terminal sheared U•U pairs of stem P4. a, Stacking and pairing alignments of the extended stem formed by C90 to C94 and G39 to G41. b, Pairing alignment of the A-minor motif A95•(C91-G40) base triple. c, Pairing alignment of the Watson-Crick C32(*anti*)-G96(*anti*) pair and the role of Mg²⁺ (green ball) in stabilizing this alignment. Note the continuous stacking from G96 to A99. d, Pairing alignment for the U47•U66 pair in the complex.



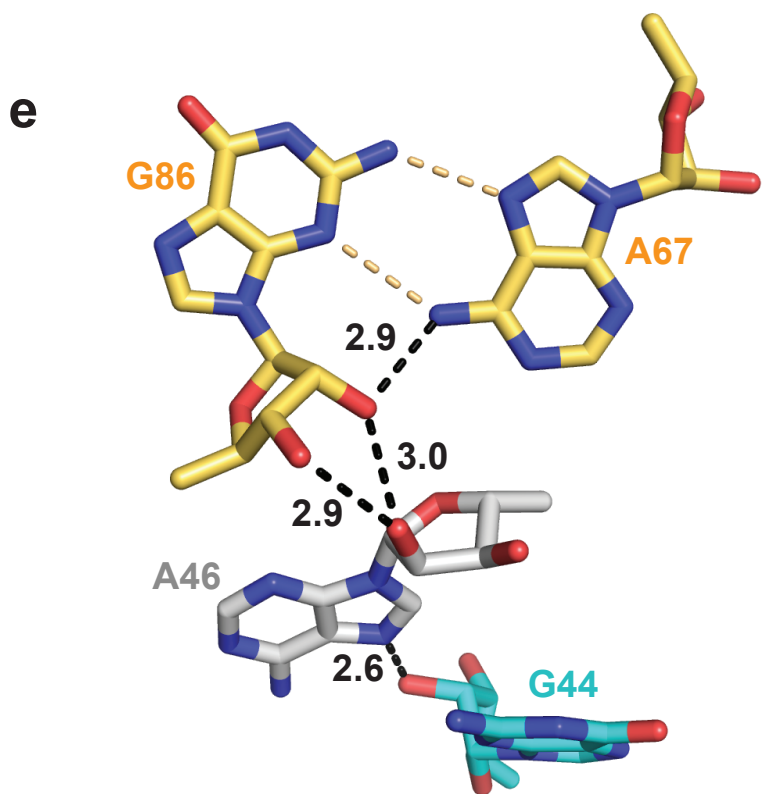
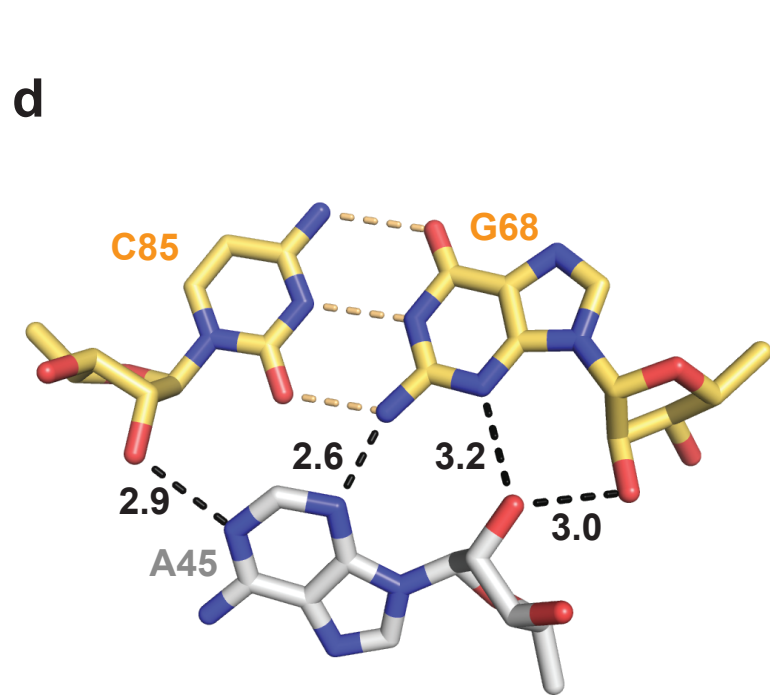
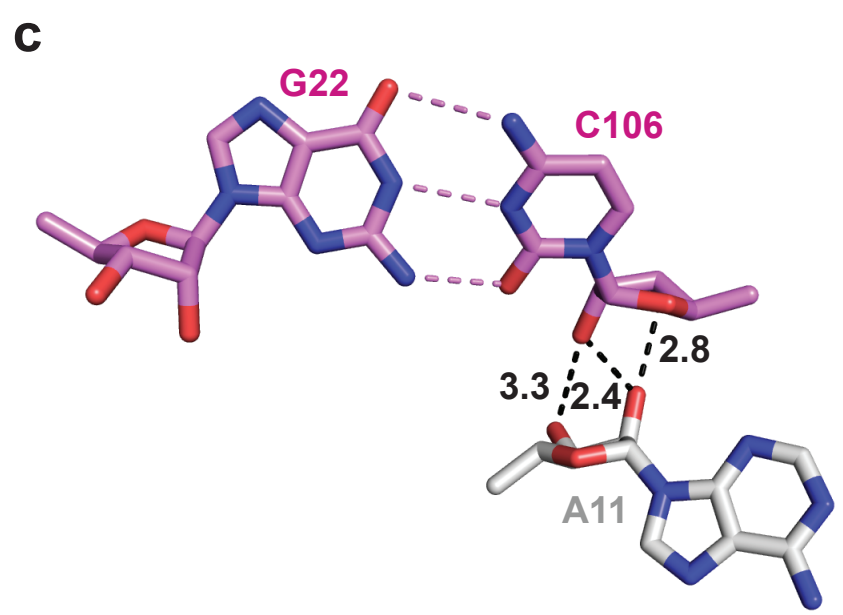
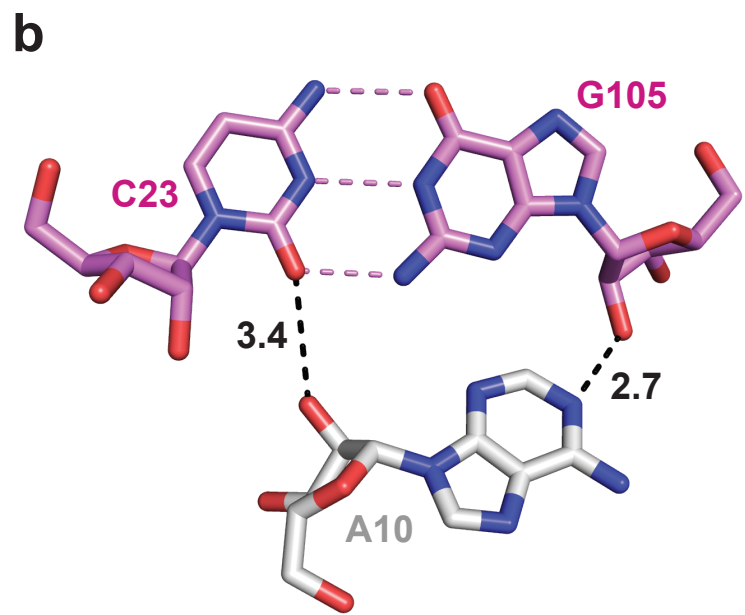
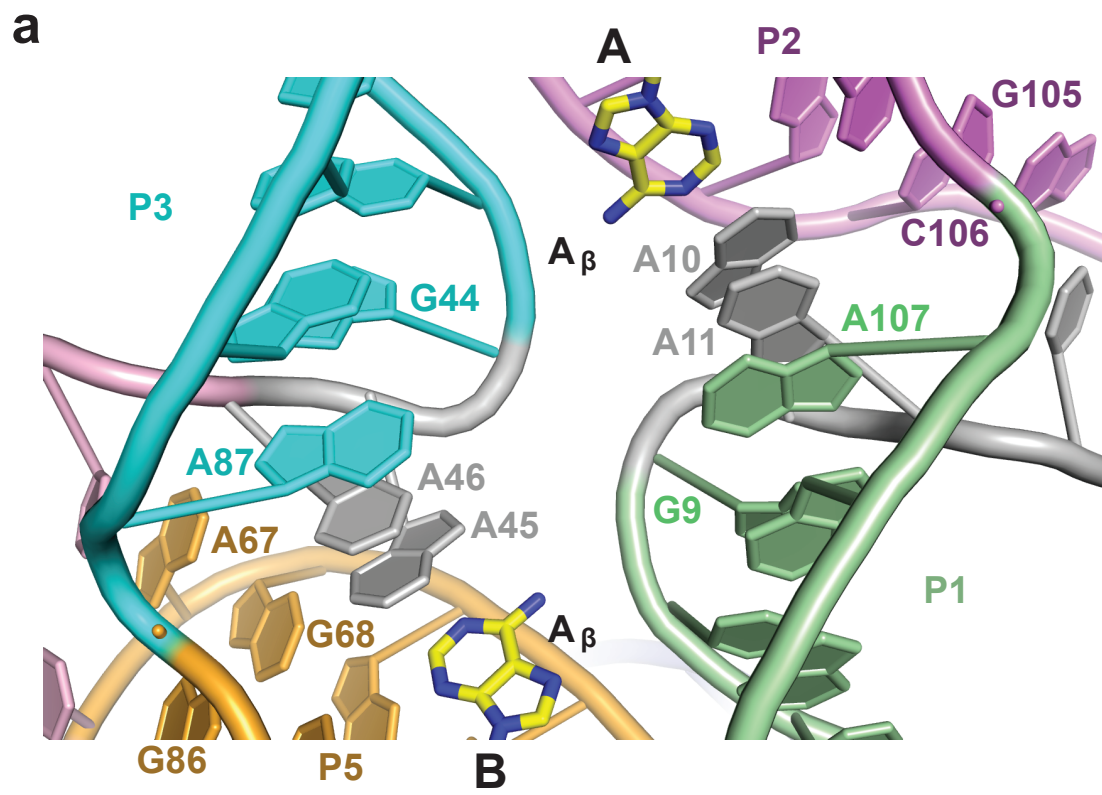
Supplementary Figure 10 | Similarities in recognition features between c-di-AMP molecules A and B bound within their respective binding pockets in the structure of the *T. tengcongensis ydaO* riboswitch bound to c-di-AMP. a, c-di-AMP molecule A (in yellow) bound within its pocket composed of stems P2 (in purple) and P3 (in cyan) and bubble (in grey) segments. b, c-di-AMP molecule B (in yellow) bound within its pocket composed of stems P1 (in green) and P5 (in orange) and pseudoknot duplex (in blue) segments. Only the bases of the RNA are shown in panels a and b, with the sugar-phosphate backbone removed in the interest of clarity.



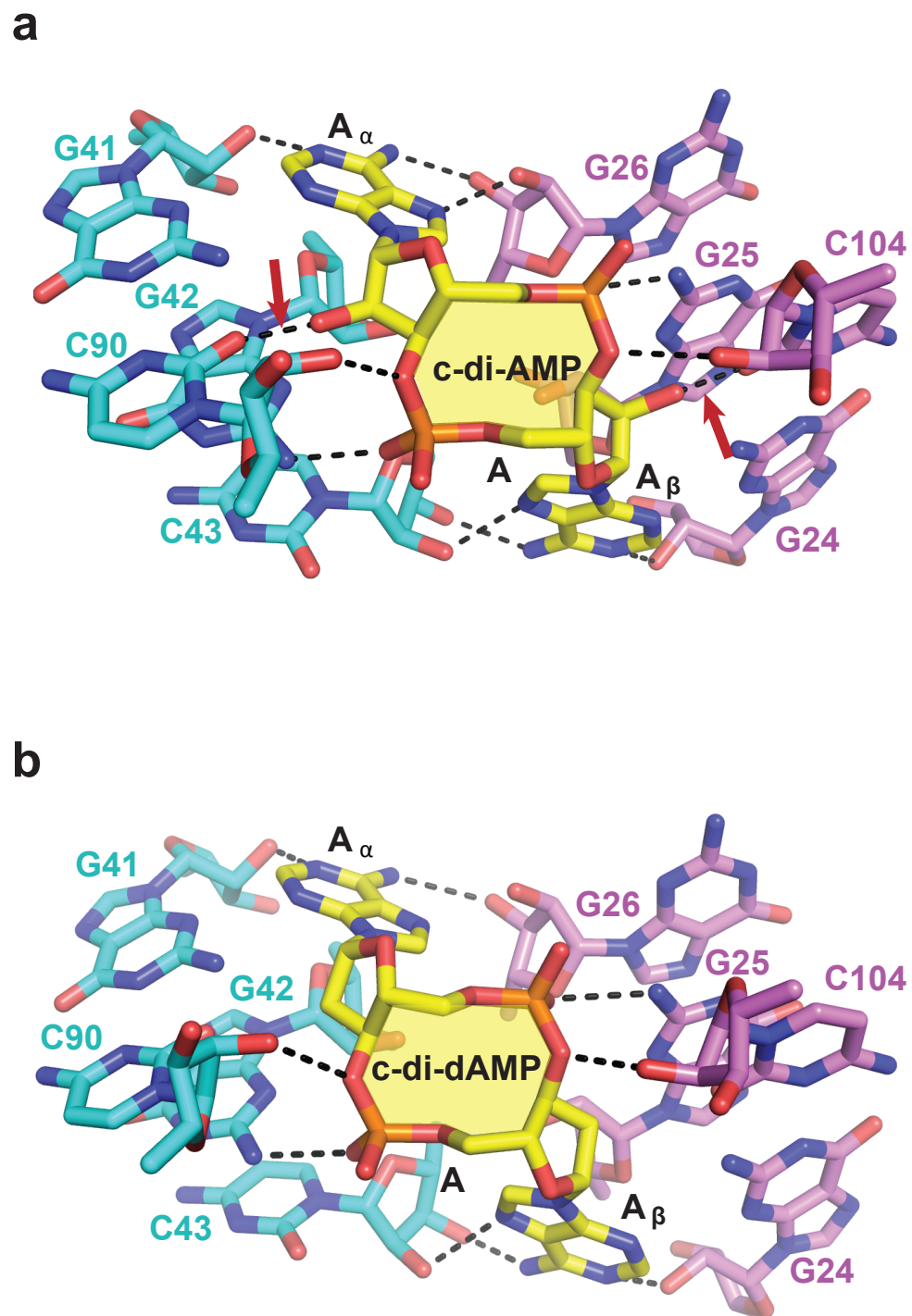
Supplementary Figure 11 | Similarities in recognition features between A β rings of c-di-AMP molecules A and B bound within their respective binding pockets in the structure of *T. tengcongensis* ydaO riboswitch bound to c-di-AMP. a, Wedge-shaped insertion of the A β ring of c-di-AMP molecule A (in yellow) between bases of stem P2 (in purple), with the A β ring stacking on A10. b, Intermolecular hydrogen bonds between the A β ring of c-di-AMP molecule B (in yellow) and the sugar rings of stems P2 (in purple) and P3 (in cyan). c, Wedge-shaped insertion of the A β ring of c-di-AMP molecule B (in yellow) between bases of stem P5 (in orange), with the A β ring stacking on A45. d, Intermolecular hydrogen bonds between the A β ring of c-di-AMP molecule B (in yellow) and the sugar rings of stems P1 (in green) and P5 (in orange).



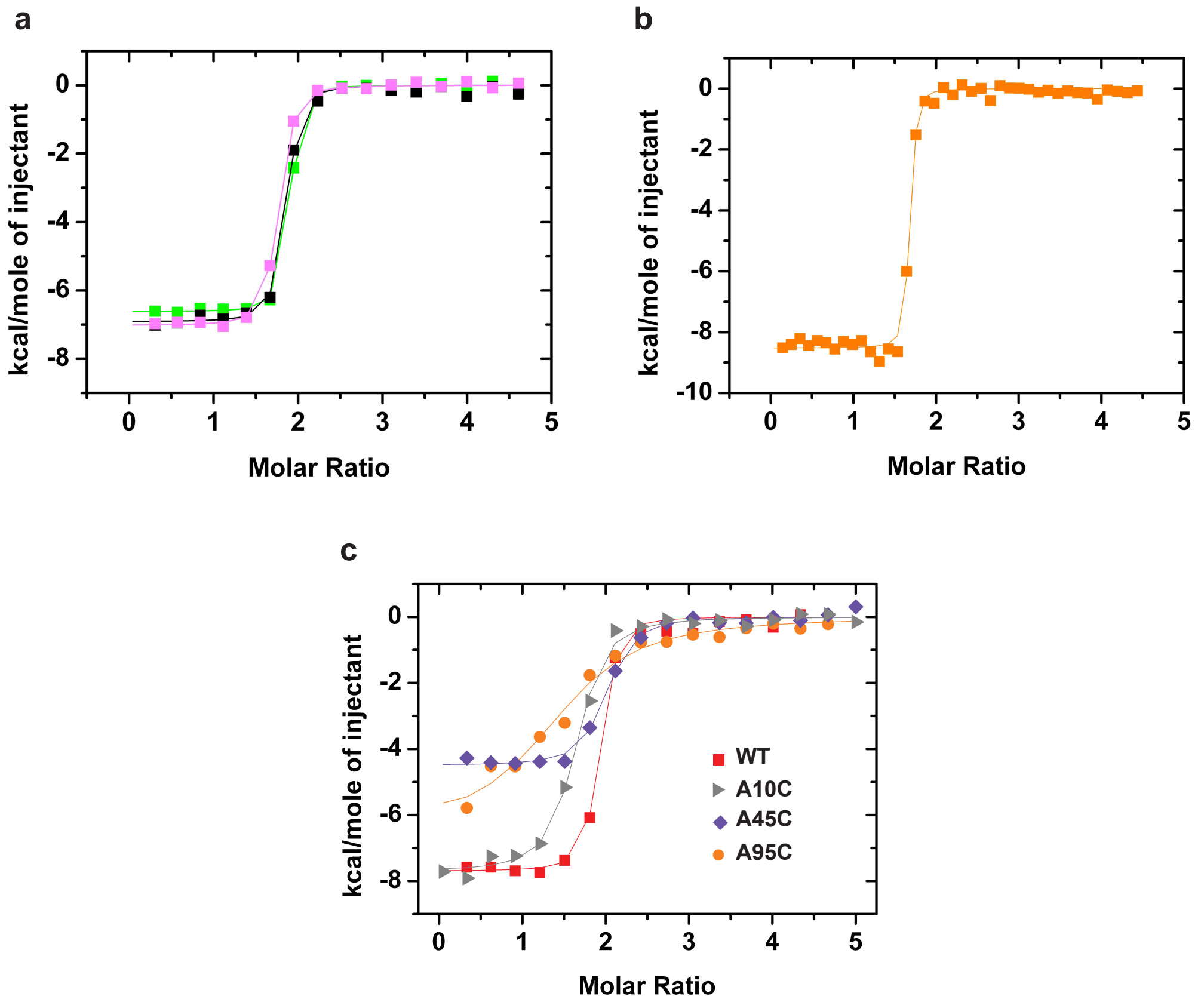
Supplementary Figure 12 | Intermolecular hydrogen bond lengths between c-di-AMP and RNA residues within the binding pocket of the structure *T. tengcongensis ydaO* riboswitch bound to c-di-AMP. The intermolecular hydrogen bond lengths are depicted in Å (heteroatom to heteroatom).



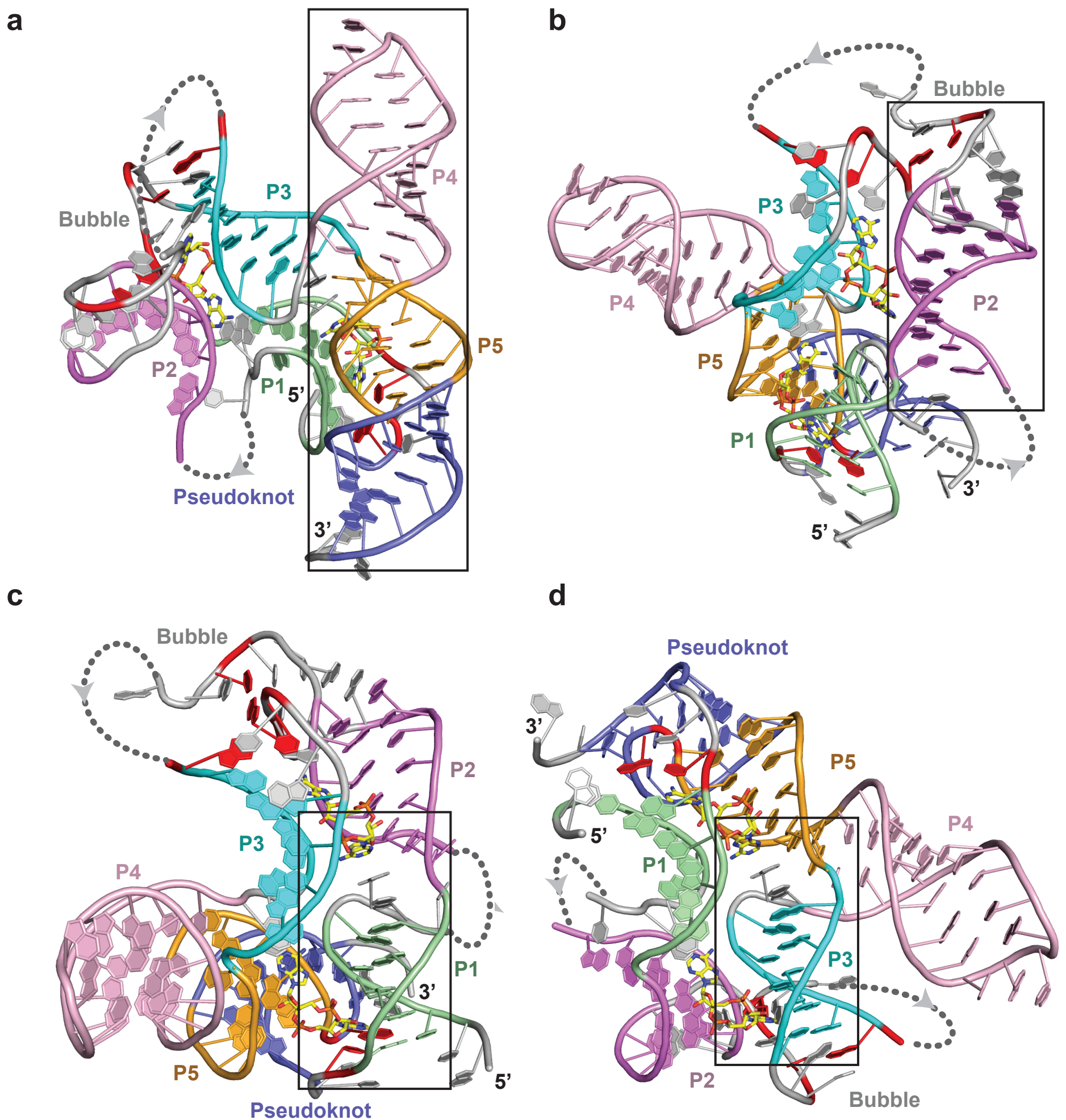
Supplementary Figure 13 | Local symmetry and pairing alignments identified in the central region of the *T. tengcongensis* ydaO riboswitch bound to c-di-AMP. **a**, Folding topology of the central region between two c-di-AMP binding pockets in the *ydaO* riboswitch complex. Junctional nucleotides A10 and A11 (in grey) continue stacking on stem P1 (in green) and form A-minor motif interaction and sugar-base recognition with stem P2 (in purple). Junctional nucleotide A45 and A46 (in grey) continue stacking on stem P3 (in cyan) and form A-minor motif interaction and sugar-base recognition with stem P5 (in orange). **b**, Pairing alignment of the A-minor motif A10•(C23-G105) base triple. **c**, Positioning of the sugar ring of A11 in the minor groove of the G22•C106 base pair. **d**, Pairing of the A-minor motif A45•(C85-G68) base triple. **e**, Positioning of the sugar ring of A46 in the minor groove of the sheared G86•A67 non-canonical pair. The hydrogen bond lengths shown in panels b to e are in Å (heteroatom to heteroatom).



Supplementary Figure 14 | Structures of *T. tengcongensis* *ydaO* riboswitch bound to c-di-AMP and c-di-dAMP. **a**, Intermolecular hydrogen bonds between c-di-AMP and the *ydaO* riboswitch, with those involving the sugar 2'-OH groups of c-di-AMP indicated by a red arrow. **b**, Intermolecular hydrogen bonds between c-di-dAMP and the *ydaO* riboswitch.

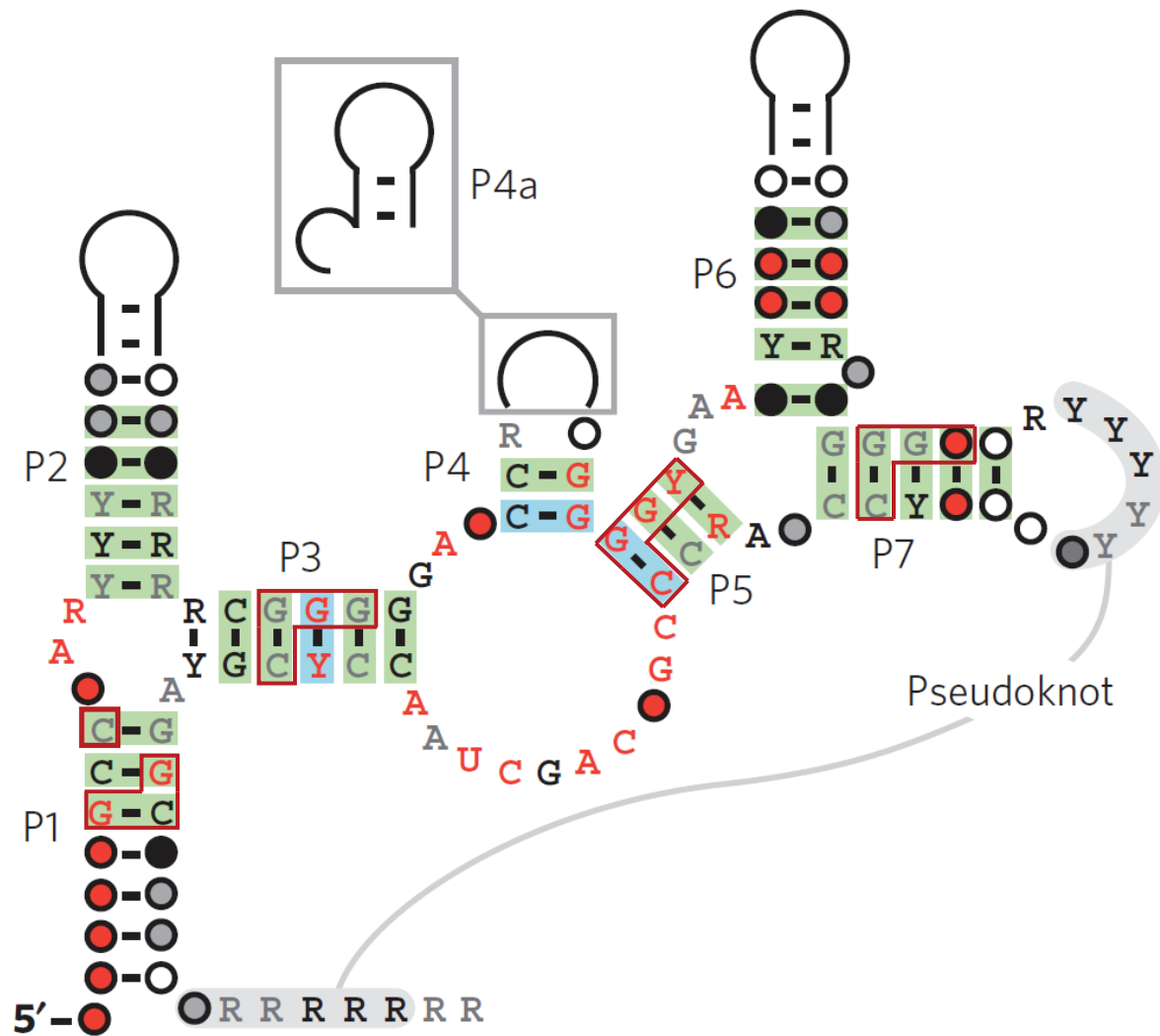


Supplementary Figure 15 | Reproducibility of ITC curves for the binding of c-di-AMP to the *T. tengcongensis ydaO* riboswitch and mutants involved in A-minor triples interaction in the *T. tengcongensis ydaO* riboswitch. **a, Superposition of three ITC curves for the binding of c-di-AMP to the *T. tengcongensis ydaO* riboswitch. **b**, ITC curve for the binding of c-di-AMP to the *T. tengcongensis ydaO* riboswitch with smaller increments of c-di-AMP added to the riboswitch. **c**, Replacement one at a time of adenines in A-minor triples involving A10, A45 and A95 by C. In panels a to c, the c-di-AMP was added gradually to mutants of *T. tengcongensis ydaO* riboswitch.**

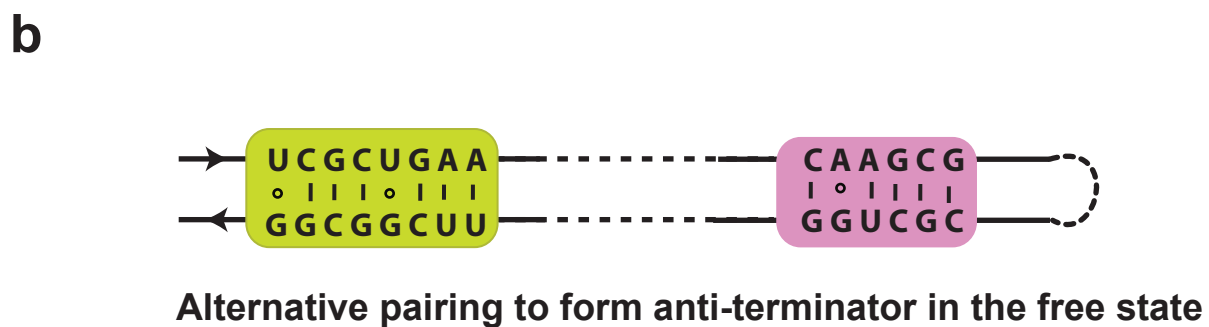
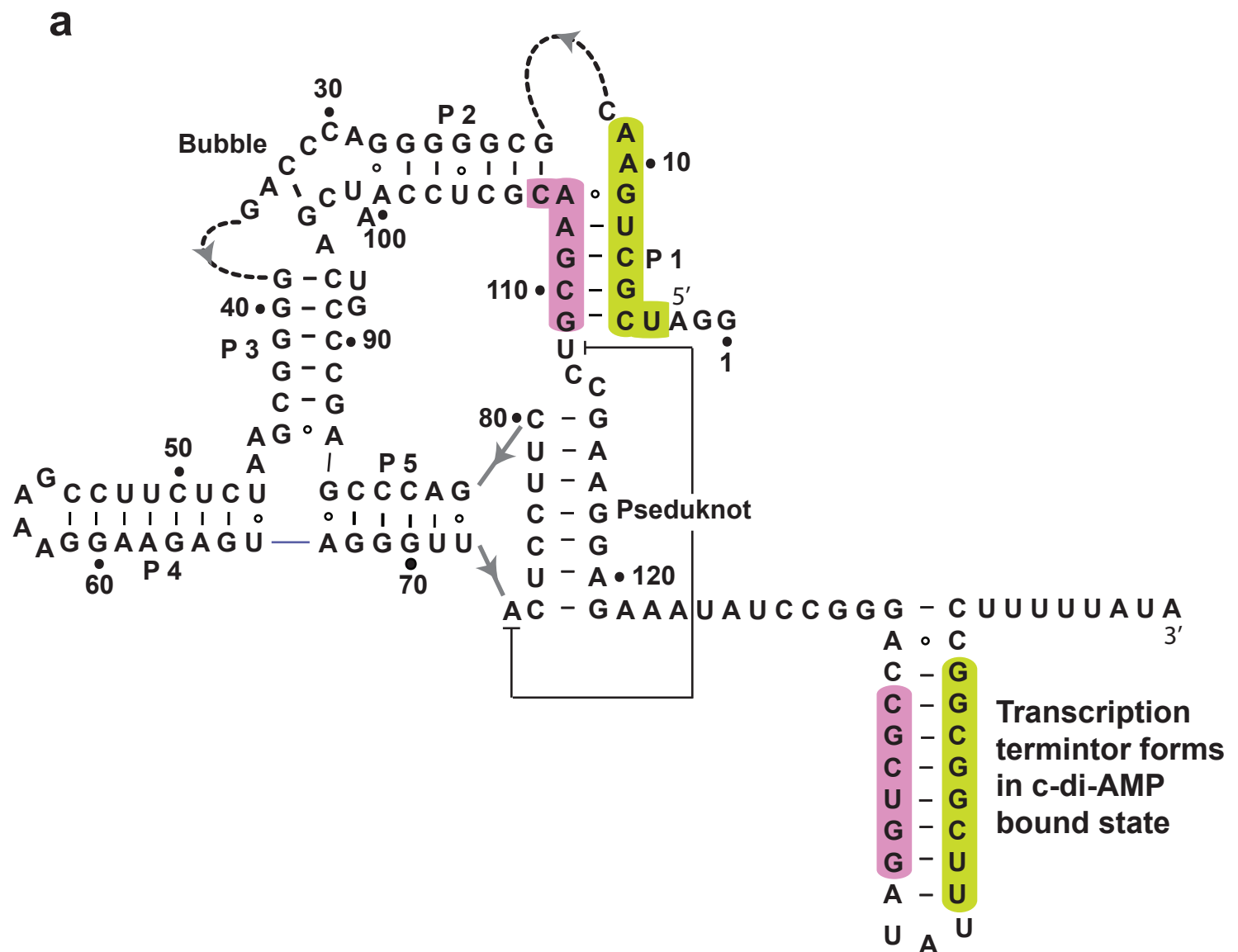


Supplementary Figure 16 | Alternate views of the crystal structure of the *T. tengcongensis ydaO* riboswitch bound to two molecules of c-di-AMP. a, This view emphasizes collinear stacking of stem P4, stem P5, and pseudoknot-derived stem (boxed segment) in the complex. **b,** This view emphasizes collinear stacking of stem P2 and elements of the zippered up bubble (boxed segment) in the complex. **c,** This view emphasizes collinear stacking of stem P1 and the adenine ring of c-di-AMP molecule A (boxed segment) in the complex. **d,** This view emphasizes collinear stacking of stem P3 and the adenine ring of c-di-AMP molecule B (boxed segment) in the complex.

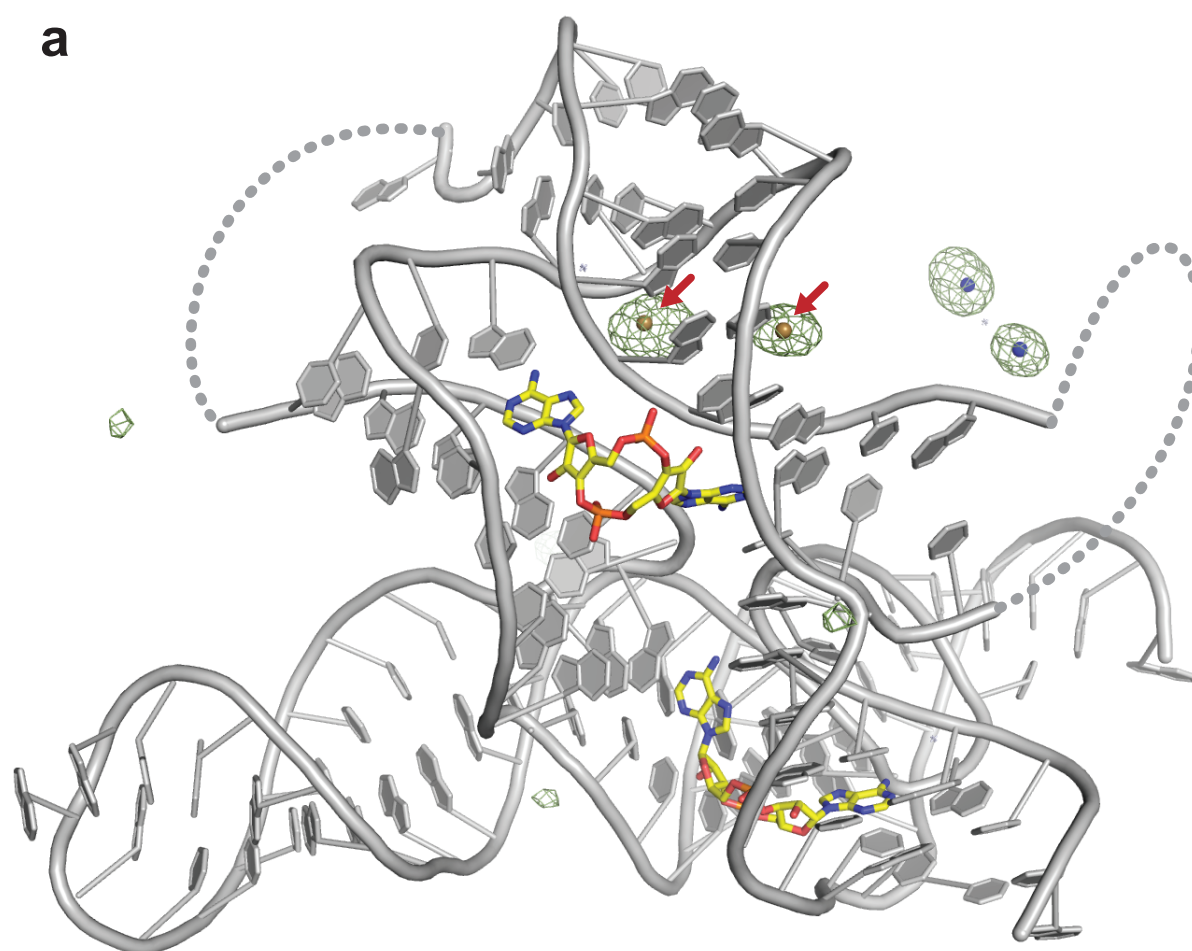
a



Supplementary Figure 17 | Labeling of binding pocket residues within the consensus sequence and secondary structure of the *ydaO* riboswitch as reported in ref. 20. Nucleotides present in greater than 97%, 90% and 75% are represented in red, black and grey²⁰. The boxed segments label binding pocket residues identified in the structure of the *T. tengcongensis ydaO* riboswitch bound to two molecules of c-di-AMP.



Supplementary Figure 18 | *T. tengcongensis* c-di-AMP *ydaO* riboswitch potentially functions through a transcription termination pathway. a, The secondary fold of the *ydaO* riboswitch in the c-di-AMP bound state. This segment contains the sensing domain and adjacent 3'-expression platform segment, a portion of which forms a transcription terminator. **b**, Alternate pairing alignment to form an antiterminator following disruption of stem P1 and the stem-loop of the terminator.



Supplementary Figure 19 | Location of two $\text{Ir}(\text{NH}_3)_6^{3+}$ binding sites in the sensing domain of the ligand-bound *T. tengcongensis* *ydaO* riboswitch. The refined c-di-AMP bound riboswitch structure based on a 2.73 Å Ir^{3+} SAD data set superposed with the anomalous Ir^{3+} map (green) contoured at 5σ level. The two bound Ir^{3+} ions are shown as brown spheres and indicated by red arrows. The blue spheres represent symmetry-related Ir^{3+} ions.